

Shear-induced adhesive failure of a rigid slab in contact with a thin confined film

M.K. Chaudhury^a and K.H. Kim

Department of Chemical Engineering, Lehigh University, Bethlehem, PA 18015, USA

Received 20 February 2007 and Received in final form 2 May 2007

Published online: 9 July 2007 – © EDP Sciences / Società Italiana di Fisica / Springer-Verlag 2007

Abstract. A rigid-glass prism (square or rectangular base, rectangular cross-section) is sheared off a thin film of silicone elastomer bonded to a glass plate by applying a tangential force at various distances above the prism/elastomer interface. At a given tangential force, the prism starts to slide on the elastomeric film. As the sliding velocity, thus the frictional force, is progressively increased, an elastic instability develops at the interface that results in the formation of numerous bubbles. These bubbles, the lateral dimension of which is comparable to the thickness of the film, move across the interface with speeds 1000 times faster than the overall sliding speed of the glass prism against the PDMS film. It is found that the glass prism continues to slide on the elastomeric film as long as the applied shear stress is less than a critical value. During sliding, however, a normal stress is developed at the interface that decays from the front (*i.e.* where the force is applied) to the rear end of the prism. When the normal stress reaches a critical value, the prism comes off the film. The critical shear stress of fracture increases with the modulus of the film, but decreases with the thickness following a square root relationship, as is the case with the removal of rigid punches from thin elastomeric films by normal pull-off forces.

PACS. 68.35.-p Solid surfaces and solid-solid interfaces: Structure and energetics – 46.50.+a Fracture mechanics, fatigue and cracks – 68.35.Np Adhesion

1 Introduction

We face many situations in which a solid object is removed from another by applying normal, shear or the combination of the two forces. If both the adherents are *ideally* rigid, and the interface is free of defects, they cannot be separated (rather fractured) from each other with any reasonable force. However, if one of the solids is deformable or coated with a thin layer of a low modulus material, then they can be separated with a finite force. An example of the above principle is the release of some biological organisms from marine vessels. Most marine organisms secrete adhesive films that interact either strongly or weakly with organic coatings. However, even when weak interaction prevails, it is not an easy task to remove the organisms from surfaces, as they maximize their resistance to release by optimizing the mechanical and geometric properties of the adhesives. Ubiquitous marine organisms, such as barnacles [1], use high-modulus adhesives, removal of which is difficult from ship hulls as they are not amenable to storing sufficient elastic energy by deformation under moderate external force. However, the encouraging finding has been that the polymeric films of low modulus and low surface energy do promote easy release. The general

mechanism underlying the release of rigid objects from soft films can be understood on the basis of the energy balance approach of Griffith [2], which was elaborated further by Rivlin [3], Gent [4] and Kendall [5]. We [6–9], as well as others [5, 10–14], examined the adhesion and separation of a rigid stud from an elastomeric film bonded to a rigid support using peeling [6, 7] and pull-off [8, 9] tests. The general observation in the pull-off test is that the critical force (f) of adhesive fracture decreases with the film thickness (h), and increases with the shear modulus (μ) as well as the work of adhesion (W_a) following a square-root relationship, *i.e.* $f \sim (W_a \mu / h)^{0.5}$. The above result, in which the typical crack length of Griffith's fracture equation is replaced by the thickness of the film is not obvious and requires some discussion. If the crack initiates from the edge of contact of a flat-ended rigid stud and a thin elastomeric film, Yang and Li [10] noted that the pull-off stress depends not only on the thickness of the film but also on the size of the stud itself. These authors presented various scenarios for pull-off stresses corresponding to various frictional boundary conditions. Only when friction vanishes at both the film-support and film-stud interface [10], the pull-off stress is independent of the size of the stud and one finds: $\sigma_{pull-off} \sim (W_a \mu / h)^{0.5}$. However, in most practical situations, the elastomeric film is bonded to the support.

^a e-mail: mkc4@lehigh.edu

In that case, application [15] of lubrication approximation to the Stokes equation of elasticity leads to an average hydrostatic stress in the thin film as $P \sim \mu v_0 a^2 / h^3$, where a is the size of the rigid stud, μ is the shear modulus and v_0 is the vertical displacement of the film. With the above definition of the pull-off stress, the elastic energy stored in the unit area of the film is $\sim \frac{\mu v_0^2 a^2}{h^3}$. At the scaling level, the fracture criterion is that this elastic energy is on the order of the work of adhesion W_a . Thus, we have the normal displacement of the film as $v_0 \sim (\frac{W_a h^3}{\mu a^2})^{0.5}$. This gives us the stress at failure as given in equation (1):

$$P_{pull-off} \sim \left(\frac{a}{h}\right) \left(\frac{W_a \mu}{h}\right)^{0.5}. \quad (1)$$

Equation (1) with the appropriate pre-factors was derived previously [10] by Yang and Li using a rigorous approach of fracture mechanics. According to equation (1), the pull-off stress is strongly dependent on the size of the stud. Why, then in practice, the size of the stud does not matter? The reason behind the pull-off stress being independent of the size of the stud is a consequence of low cohesive stress and the resulting elastic instability at the interface [6, 8, 9, 14–19]. To illustrate the point, let us consider a stud of diameter 1 cm being pulled off an elastomeric film of 100 μm thickness and 1 MPa elastic modulus with a work of adhesion about 40 mJ/m². In this case, the required pull-off stress would be about 2 MPa according to equation (1), which is considerably larger than the stress (~ 100 KPa) at which the interface cavitates [6, 18] (perhaps caused by stress-activated growth of density fluctuation or due to pre-existing defects). Interfacial cavitation, and the subsequent minimization of the shear and longitudinal deformation energies in the film, lead to a wavy undulation of the interface [8, 9, 18, 19] (see also the appendix). The only length scale in the problem is the thickness of the film that determines the wavelength of instability. The wavy segments can be looked upon as individual cracks so that the critical pull-off stress is

$$\sigma_c \sim \sqrt{\frac{W_a \mu}{\lambda}}, \quad (2)$$

where λ is the wavelength of instability. Since λ scales linearly with thickness (h), we have [9, 15–19]:

$$\sigma_c \sim \sqrt{\frac{W_a \mu}{h}}. \quad (3)$$

Recent experimental studies [8, 9] confirmed the validity of equation (3). While, based on both theoretical and experimental results, the pull-off behavior of a rigid punch from a thin confined film is now well understood, no systematic study has been performed so far to determine what would cause a rigid punch to come off a thin film when a shear force is applied. In practical settings, the shear force is applied by pushing the rigid stud with a force applied parallel to the interface. It is expected that the prism would only slide if the force is applied in the plane

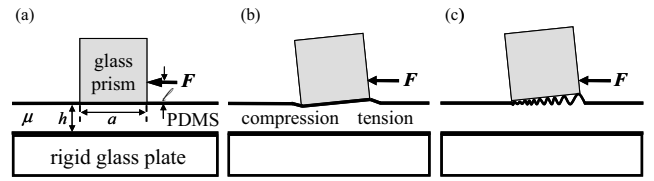


Fig. 1. (a) A rectangular glass prism (10 mm \times 10 mm \times 6 mm) is sheared off a thin film of PDMS (polydimethyl siloxane) rubber bonded to a glass plate. The rectangular glass prism was prepared by cutting a borosilicate glass plate (ACE Glass, USA) using a fine glass grinder. The root mean square roughness of the glass prism was found to be 9 nm over an area of 20 μm^2 using an atomic force microscope (AFM, Digital Instruments, USA). The force F is applied at a distance of 1 mm (ℓ) above the glass-film the interface. A torque generated by the force tries to open a crack near the edge where the force is applied. (b) This figure shows that hydrostatic tension is generated on one edge of contact accompanied with a hydrostatic compression on the other. (c) This figure presents a (somewhat exaggerated) scenario in which an elastic instability leads to the development of bubbles at the interface. These bubbles increase the compliance of the film, because it allows localized deformations.

of the prism-substrate interface. However, if the force is applied at a plane higher than the interface, the prism would come off at a critical stress. This is the situation that we investigate in this paper.

2 Model system

The particular situation that we are interested in is shown in Figure 1a, where a force is applied to a prismatic stud at a distance ℓ above the interface. We expect the stud to slide on the elastomeric film as long as the applied force F is larger than the static shear force. However, as the external force is not applied right at the interface but slightly above it, an external torque is generated, which must be balanced by an internal torque at the interface. This balance of torque can be written as

$$F \cdot \ell = w \int \sigma_n x dx, \quad (4)$$

where w is the width ($\approx a$) of the stud, σ_n is the normal stress and x is the distance from the rear edge of the film-prism interface. In what follows next, we consider two different scenarios. The first scenario involves treating the film as fully confined, whereas the second one relaxes the confinement of the film by means of an elastic instability.

If we consider that the PDMS film is fully confined, *i.e.* the stress state in the film is hydrostatic, the vertical displacement (v) of the film is given by the lubrication solution [15] of the elastic Stokes equation (see also the appendix) as follows:

$$v = -\frac{h^3}{12\mu} \frac{d^2 P}{dx^2}. \quad (5)$$

The vertical displacement of the film is related to the inclination of the prism and is given by

$$v = v_o \left(\frac{x}{a} \right) + C_1. \quad (6)$$

Here, v_o and C_1 are constants to be determined.

Equation (5) is integrated in conjunction with equation (6) with the following boundary conditions. The pressure is maximally tensile at $x = a$ and maximally compressive at $x = 0$. Furthermore, the net force in the vertical direction, *i.e.* the integral of the pressure over the whole surface of contact, is zero. Under these assumptions, the pressure profile at the interface is given by

$$P = -\frac{\mu v_o}{2h^3} \left(\frac{4x^3}{a} - 6x^2 + a^2 \right), \quad (7)$$

with the maximum tensile pressure at $x = a$ as

$$P_{max} = \frac{\mu v_o a^2}{2h^3}. \quad (8)$$

Integration of equation (4), where the normal stress σ_n is replaced by P , leads to the following equation:

$$\sigma_s = \left(\frac{a}{5\ell} \right) P_{max}. \quad (9)$$

The maximum stress can be obtained using the usual energy balance principle of fracture mechanics, in which we first find the total energy of the system by summing up the elastic and surface energy and setting the derivative of this energy with respect to the crack length equal to zero. The total energy of the system per unit width can be expressed as

$$U = \int_0^a dx \int_0^{v_o} P dv - W_a a, \quad (10)$$

where the first term is the elastic energy and the second term is the adhesion energy. Using equations (6-8), equation (10) can be written as

$$U \sim \frac{\mu v_o^2 a^3}{h^3} - W_a a. \quad (11)$$

Setting $\frac{\partial U}{\partial a} \Big|_{v_o} = 0$, and making use of equation (8), we obtain

$$P_{max} \sim \left(\frac{a}{h} \right) \sqrt{\frac{W_a \mu}{h}}. \quad (12)$$

Equation (12) is of the same form as that obtained for the pull out of the stud with an uniform normal force as discussed above (Eq. (1)). However, there is a problem with the above analysis. It has been found that during the separation of the prism from PDMS film, a fingering instability [20] always develops at the line of contact, which suggests that the film is more compliant near the contact line region than would be expected for a fully confined film. In this case, the loss of the interfacial contact is first controlled by the increase of the amplitude of the fingers,

and then a catastrophic crack growth ensues at a later stage.

It has been further observed experimentally that as the fingers that develop at the contact line elongate, they break down in the form of bubbles that travel the interface from one end towards the other. Thus the compliance of the film is expected to increase not only near the contact line, but throughout the entire area of contact. The situation is now similar to that of a rigid plate that is connected to a horizontal base via a series of springs and is being lifted from end one with a force. All the springs elongate, with the elongation increasing linearly from its rear end to where the force is applied. The net result is that a concentrated compressive force generates on the rear end of the plate. Using the above scenario (see also Fig. 1b), we assume that the tension is maximum (σ_n^*) at $x = a$, but it varies linearly across the interface (see the appendix), *i.e.*

$$\sigma_n = \sigma_n^* \left(\frac{x}{a} \right). \quad (13)$$

In order to satisfy the condition that there is no net normal force on the slab, a localized compressive force ($\sigma_n^* a/2$) needs to act at $x = 0$ per unit width of contact. Substitution of the expression (Eq. (13)) of normal stress in the torque balance equation, we have the shear stress as

$$\sigma_s = \sigma_n^* \left(\frac{a}{3\ell} \right). \quad (14)$$

Following the energy minimization procedure as before, and using an expression [15] for the relationship between normal force σ_n and normal displacement v as $\sigma_n \sim \mu v/h$ (see the appendix), we expect the maximum normal stress to adhesive fracture to be

$$\sigma_n^* \sim \sqrt{\frac{W_a \mu}{h}}, \quad (15)$$

which is of the same form as equation (3) obtained for pull-off experiments. Thus, we have two possible situations. If the film is in a confined state, equations (9) and (12) suggest that the critical shear stress at fracture is

$$\sigma_s^* \sim \left(\frac{a^2}{h\ell} \right) \sqrt{\frac{W_a \mu}{h}}. \quad (16)$$

On the other hand, if an elastic instability ensues at the interface, equations (14) and (15) suggest that the critical shear stress at fracture is

$$\sigma_s^* \sim \left(\frac{a}{\ell} \right) \sqrt{\frac{W_a \mu}{h}}. \quad (17)$$

While the critical shear stress at fracture goes as $\mu^{1/2}$ in both the models, it depends on thickness more strongly (*i.e.* $h^{-1.5}$) in a fully confined film (Eq. (16)) than that ($h^{-0.5}$) for a film that relieves the confinement via elastic instability (Eq. (17)). One goal of this work is to verify which mechanism underlies the shear induced adhesive failure in thin elastic film.

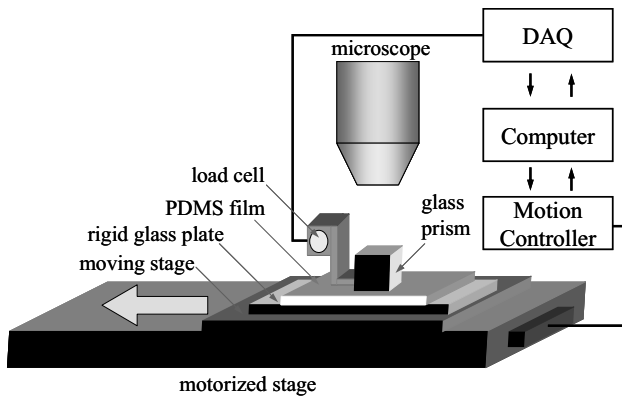


Fig. 2. Schematic of the experimental apparatus. A silanized glass prism ($10\text{ mm} \times 10\text{ mm} \times 6\text{ mm}$) is placed on a thin PDMS film bonded to a glass slide. The glass slide is itself placed on a moving stage, the movement of which is controlled by a motorized stage controlled by a motion controller and computer. The motorized stage is the Nanostep Motorized System (model 17NST103, Melles Griot, USA), velocity variation of which is controlled from $0.5\text{ }\mu\text{m/s}$ to 5 mm/s . A firmly held beam load cell (model LBB300, Futek Advanced Sensor Tech., USA) is used to measure the shear force. DAQ (model NI USB-9215A, National Instruments, USA) is used to collect data. Interfacial fracture was observed with a microscope (model CFM-2 Microscope Video Lenses, Infinity Photo-Optical com., USA) using either a CCD camera (model KP-D20BU, Hitachi, Japan) with a video recorder or a high speed camera (model Motion-Pro, Redlake, USA). A sharp edge made of steel protrudes from the load cell, which makes contact with the glass prism at an adjustable distance from the interface of contact. For most measurements, this distance was set to be about 1 mm . As the glass slide starts moving, the prism exerts a force on the sharp edge, which is recorded by the load cell and the computer. The interface of the contact is viewed and video-taped with a high-speed camera.

3 Experiment

We performed the following experiments. A glass prism is sheared on thin films of crosslinked polydimethylsiloxanes of various elastic moduli by applying a force at a pre-set distance on the prism above the prism/elastomer interface (Fig. 2). The specific dimensions of the prisms and the point of application of the stress are given in the legends of various figures (Figs. 2, 3, 6 and 8) summarizing the results of the specific experiments. However, in most experiments the dimension of the prism was $10\text{ mm} \times 10\text{ mm} \times 6\text{ mm}$ and the shear force was applied at a distance of 1 mm about the prism-PDMS interface. In order to reduce specific interactions at the interface, the glass prism was silanized with hexadecyl siloxanes. After placing the glass prism on a PDMS-coated glass slide, it was translated laterally at various speeds using a motorized stage. The glass prism was rested against a sharp blade connected to a beam load cell, which measured the shear force as the PDMS-coated glass slide moved relative to the glass plate.

The experiment could be carried out in one of two ways. In the first method, the prism could undergo a

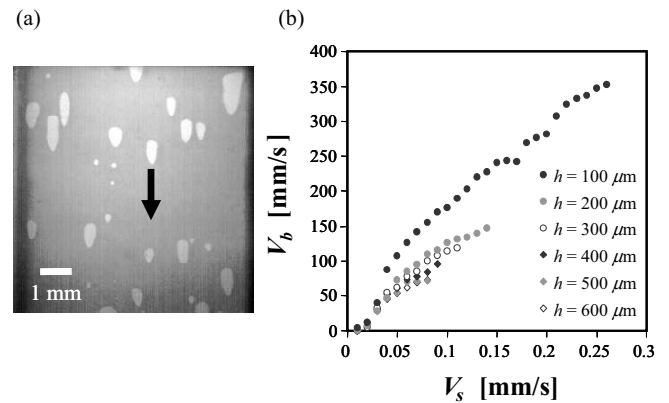


Fig. 3. (a) Video micrograph of interfacial bubbles observed during shear experiments. The dimension of the prism was $10\text{ mm} \times 10\text{ mm} \times 6\text{ mm}$ and the shear force was applied at a distance of 0.5 mm above the interface. Interfacial bubbles moving along the direction of the arrow. Film thickness, $h = 400\text{ }\mu\text{m}$ and shear modulus of the film, $\mu = 1.6\text{ MPa}$. (b) Velocity of bubbles is nearly 1000 times faster than the relative sliding speed between the rectangular prism and the PDMS-coated glass slides.

steady sliding against the PDMS film. Here, we observe that the prism continues to slide on the PDMS film without ever coming off (unless a defect is encountered) at low sliding speeds. After performing the experiment at increasing sliding speeds, a critical speed is reached, when the prism readily comes off the film. We are interested in finding out the critical speed at which the prism just comes off the thin film. Identification of this critical condition is rather cumbersome using the above method of steady-state sliding as numerous experiments need to be conducted. We thus used a different approach, in which the movement of the stage is programmed to slide for a small duration of time (2 seconds) and then the sliding velocity is increased incrementally (0.002 mm/s). This process is repeated till the sliding speed reaches the critical value at which fracture occurs at the interface.

4 Results and discussion

4.1 Elastic instability and movements of bubbles at the interface

The typical behavior of the shear stress/sliding velocity profile as obtained from the sliding experiments is discussed below (see Fig. 6). However, before that discussion, we first describe some details of the elastic instability that develops at the punch/film interface. At very low sliding speeds the cube seems to slide against PDMS smoothly; however as the sliding speed increases, the torque generated in the cube tends to lift it slightly at the frontal edge causing an elastic fingering instability (not shown in Fig. 3). As these fingers penetrate the prism/film interface, they break up as small bubbles.

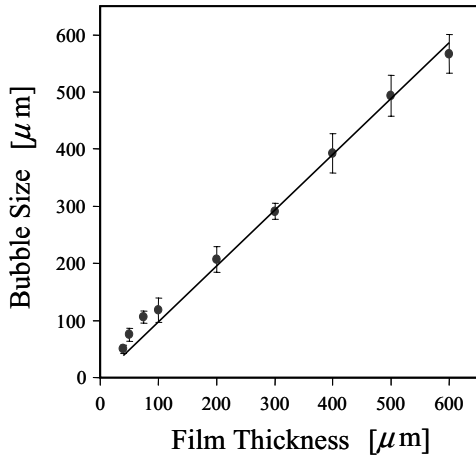


Fig. 4. The lateral size of the interfacial bubble is of the same size as the thickness of the PDMS film. Here the error bar corresponds to the distribution of the size of the bubbles.

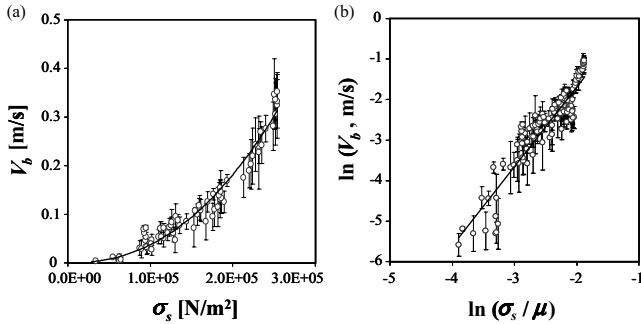


Fig. 5. (a) The bubble velocity V_b is plotted against the shear stress σ_s for a PDMS elastomer of elastic modulus 1.6 MPa. The relationship between bubble velocity and shear stress is found to be: $V_b = 2 \times 10^{-13} \sigma_s^{2.28}$ with a correlation coefficient of 0.92. (b) The bubble velocity is plotted against σ_s/μ on a logarithmic scale. Here data from PDMS of various moduli (0.3, 0.4, 0.9, 1.6 and 3.2 MPa) are combined in one plot. The equation describing this plot is: $\ln(V_b) = 1.97 \ln(\sigma_s/\mu) + 2.25$ with a correlation coefficient of 0.87.

These bubbles then move from the frontal towards the rear edge with speeds that are nearly 1000 times faster than the actual sliding speeds of the prism.

In the case of the sliding of a rigid object over soft elastomer it is well known that a detachment wave, *i.e.* Schallamach wave [21], propagates from the rear end to the frontal end of the slider. These Schallamach waves are due to surface buckling instability that occurs in thick films. The bubbles, on the other hand, move along the direction of sliding and they occur only in thin confined films. It appears that formation of these bubbles is unique to confined systems, although they share the features of Schallamach waves [21, 22] and slip pulses [23] in that the propagations of all of these are driven by the gradient of shear strain energy.

One interesting observation is that the size of the bubbles is of the similar magnitude as the thickness of the film as shown in Figure 4, a fact that we will use later in deriv-

ing the speeds of the moving bubbles. In a recent elegant review, Baumberger and Caroli [24] discussed the propagation of slip pulses for a thick gel sliding against a rigid substrate. These authors proposed that the velocity of the slip pulse is the ratio of a collective diffusion coefficient D and the mesh size of the gel network. D is expressed as $\mu\xi^2/\eta_s$, where μ is the shear modulus of the network, ξ is its mesh size, and η_s is the viscosity of the solvent in the gel. Recently Brochard-Wyart and de Gennes [25] provided a theoretical justification of the above Baumberger-Caroli equation, by equating the driving force for the propagation of slip pulse and the frictional force it experiences. It should be noted that the Baumberger-Caroli's expression for the slip velocity, which also manifests in other stick slip experiments [26–28] as a ratio of the mesh size to mesh relaxation time, is a material velocity. In our experiment, the bubble velocity being strongly dependent on the slip velocity (Fig. 4), and thus the applied shear stress (Fig. 5), is not strictly a material velocity. Here we present an approximate analysis that accounts for the energetics of bubble propagation in a confined geometry. The movement of the bubbles is related to the motion of shear stress dislocations, the driving force of which is provided by the shear strain energy in the film. The mechanics of the situation may be understood as follows. Let us consider an unstrained elastomeric film/solid interface where insertion of a bubble creates a symmetric strain field in the elastomeric film around the bubble. If a shear strain is now imposed, the combination of this new and the previously present strain fields creates a net asymmetric strain field, the effect of which is to open a crack in the front of the bubble but to close the crack behind it. As the bubble moves, the shear strain in the film around the bubble is relaxed. In the absence of interfacial adhesion hysteresis, the associated elastic energy is dissipated in the cyclic viscoelastic deformation in the rubber. As the bubble moves laterally, the region ahead of it is deformed, but the region behind is relaxed. In a static situation, the elastic energy stored around a bubble is $\sim \mu b^3$, where b is the size of the bubble. The movement of a bubble is conceptually equivalent to periodic processes of the growth of the bubble from zero radius to its final dimension and then back to zero radius. At the scaling level the rate of work done in this process is $\mu(db^3/dt)$, which is also same as the modulus times the rate of volume excursion by a single bubble per unit time $\sim \mu b^2 V_b$. When a perfectly elastic rubber undergoes a cyclic deformation, no energy is lost in the whole process. However, in a real rubber, a fraction of this energy is dissipated, which is estimated following a method of Shanahan and Carré [29] as $(V_b/V_{b0})^\alpha$, where V_b is the bubble velocity; V_{b0} and α are constants. The rate of energy dissipation is then,

$$\frac{dE}{dt} \sim \mu b^2 V_b \left(\frac{V_b}{V_{b0}} \right)^\alpha. \quad (18)$$

Suppose that during the propagation of a bubble, a length χ of the rubber relieves the shear strain energy. The elastic energy stored along the length $\ell - \chi$ of the rubber of

width b (*i.e.* that of a bubble), is

$$U = \frac{\sigma_s^2 b h (\ell - \chi)}{\mu}. \quad (19)$$

The rate of change of this energy per unit extension of χ is

$$-\frac{\partial U}{\partial \chi} = \frac{\sigma_s^2 b h}{\mu} \quad (20)$$

$-\frac{\partial U}{\partial \chi}$ is the driving force for bubble motion. Since the rate of work done ($\frac{dE}{dt}$) in the movement of the bubble is equal to energy dissipation, we have

$$\frac{\sigma_s^2 b h V_b}{\mu} \sim \mu b^2 \left(\frac{V_b^{1+\alpha}}{V_{b0}^\alpha} \right). \quad (21)$$

We observe experimentally (Fig. 4) that the dimension of the bubble is on the order of the thickness of the PDMS film. This is a consequence of elastic instability in the film and may be understood according to a simple scaling argument given in references [8,9,18], in which we minimize the elastic and surface strain energy of the film (see the appendix for details) to obtain $\lambda \sim h$. That is to say that there is one characteristic wavelength for which the sum of the longitudinal and transverse strain energy is minimum. This wavelength describes the width of the finger, which, in reality, is about four times the film thickness as has been described in references [7,9,16,19]. In our experiments, as such a finger elongates, it breaks down in the form of smaller bubbles that move across the interface. Why these fingers produce bubbles that are four times smaller than its own width is not clear to us. However, we expect that the bubble size would be proportional to the thickness of the film since it is related to the width of the fingering instability, as found experimentally (Fig. 4). Since the bubble size is on the order of the film thickness, equation (21) can be simplified to

$$V_b \sim V_{b0} \left(\frac{\sigma_s}{\mu} \right)^{\frac{2}{\alpha}}. \quad (22)$$

For a linear viscoelastic rubber, we may take $\alpha = 1$. Hence the bubble velocity is

$$V_b \sim V_{b0} \left(\frac{\sigma_s}{\mu} \right)^2. \quad (23)$$

The bubble velocities obtained with PDMS films of various thicknesses but with a given shear modulus (1.6 MPa) do indeed increase nearly quadratically (Fig. 5a) with σ_s . Figure 5b summarizes the bubble velocities obtained with PDMS films of various elastic moduli, where V_b is plotted against σ_s/μ on a log-log plot. Although there is some scatter in this plot, it shows that V_b varies with σ_s/μ with a power law exponent close to 2 in conformity with equation (23). From the intercept of this plot, the pre-exponential velocity V_{b0} is estimated to be about ~ 10 m/s, which is in the vicinity of the shear wave speed (~ 30 m/s) of a rubber. Considerable amount of scatter

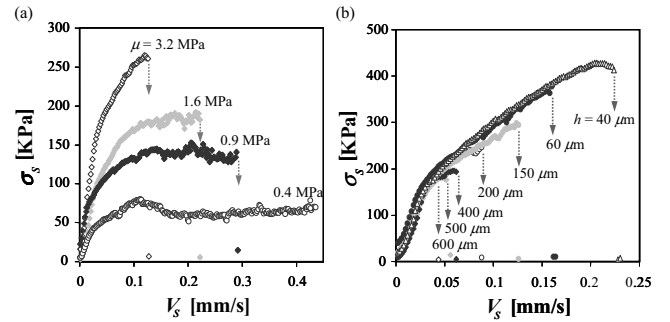


Fig. 6. (a) Shear stress of a silanized glass prism sliding against thin ($100 \mu\text{m}$) PDMS films of various shear moduli. (b) Shear stress of a glass prism sliding on PDMS films of various thicknesses, but with constant shear modulus ($\mu = 3.2$ MPa). Arrows represent the critical shear stress at which the prism comes off the film. In these experiments a $10 \text{ mm} \times 10 \text{ mm} \times 6 \text{ mm}$ prism was used whereas the force was applied at a distance of 1 mm above the prism-PDMS interface.

seen in Figure 5b is partly due to the fact that a distribution of bubble velocities at a given shear stress results from a distribution of bubble sizes. Furthermore, V_{b0} may itself depend weakly on the shear modulus μ . Understanding the precise nature of V_{b0} , its possible dependence on μ , and why the energy dissipation per deformation cycle scales as V_b/V_{b0} require a more detailed model than that invoked here. Furthermore, another important detail has been ignored here. As the bubble moves from the region of higher hydrostatic tensile pressure to a region of lower one, the size of the bubble is reduced somewhat, which also increases the interfacial adhesion. Postponing a detailed analysis that should take into account the factors outlined above to the future, here we concentrate on what roles do the bubbles play in the shear fracture of the rigid stud from the thin PDMS films.

When a fully confined film experiences a normal force in the absence of cavitation bubbles, it cannot afford a large scale Poisson contraction. As the bubbles are formed as a result of an elastic instability, they allow lateral Poisson contraction at a local level. The bubbles, thus, increase the compliance of the PDMS film, so that the normal stress along the interface is linearly proportional to the vertical displacement [8,18] of the film (see appendix). With the rigid slider, this translates into the normal stress varying linearly across the film as indicated in equation (13).

4.2 Shear stress/sliding velocity profiles

The shear stress/velocity profiles of the glass prism on several PDMS films are shown in Figure 6. Figure 6a shows these profiles for a $100 \mu\text{m}$ thick PDMS film of various moduli, whereas Figure 6b shows these profiles for a 3.2 MPa film of various thicknesses.

Note (Fig. 6a) that the prism does not always come off a low-modulus (0.4 MPa) film, irrespective of the sliding speed. If the shear stress saturates at a low value so that

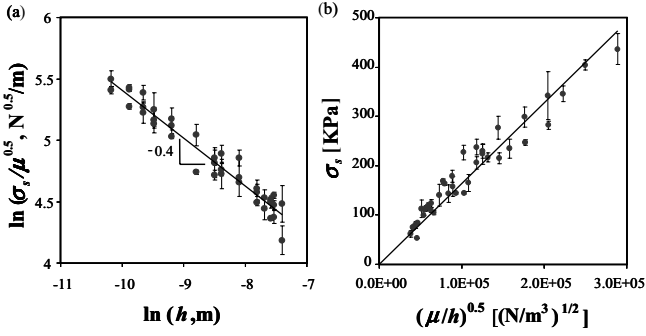


Fig. 7. The relationship between critical shear stress and the modulus as well as the thickness of PDMS films.

not enough normal stress is generated at the interface, the prism does not detach from the film as is the case with the low-modulus PDMS. However, for films of shear modulus 0.9 MPa to 3.2 MPa, the glass prism indeed separates at critical sliding velocities.

Figure 6b shows that the envelope of the shear stress/velocity profiles for PDMS films of various thicknesses superimpose onto each other. The critical shear stress at which the prism comes off the film also decreases with the film thickness as expected. In order to verify whether this critical shear stress decreases with thickness as $h^{1.5}$ (Eq. (16)) or as $h^{0.5}$ (Eq. (17)), we plotted $\sigma_s/\mu^{0.5}$ vs. h on a log-log scale (Fig. 7a). The slope of the resultant regression line is 0.40, which suggests that equation (17) is a better descriptor of the experimental data than equation (16). When we plot σ_s vs. μ/h on a log-log scale (not shown here), the slope (0.44) of the resultant line is even closer to the exponent (0.5) predicted by equation (17).

Figure 7b shows a plot of the critical shear stress as a function of $(\mu/h)^{1/2}$, which has a correlation coefficient of 0.92. Although the derivation of equation (17) ignores the numerical pre-factors, we made a crude estimate of the work of adhesion W_a with this equation using the data of Figure 7b and the value of $a/\ell \sim 10$. The work of adhesion, W_a , is thus found to be about 28 mJ/m², which is lower than the typical values of the work of adhesion (40–50 mJ/m²) for PDMS against hydrocarbon surfaces [7]. In the absence of a precise equation for the critical shear stress of fracture, all that can be said now is that the work of adhesion obtained from the shear fracture measurement is in the vicinity of the value expected for van der Waals (dispersion) interactions.

While this study was primarily designed to investigate the dependence of the failure stress on the modulus and the thickness of the polymeric coating, we also investigated how the failure shear stress depends on the geometric length scales a and ℓ (Eq. (17)). The data summarized in Figure 8 indeed show that the failure stress decreases with ℓ and increases with a , although not strictly linearly as anticipated from equation (17).

Thus, before carrying out further analysis of these data, we introduce a correction to equation (17) by taking into account an energy release term due to the shear deformation in the film. The total energy release rate is

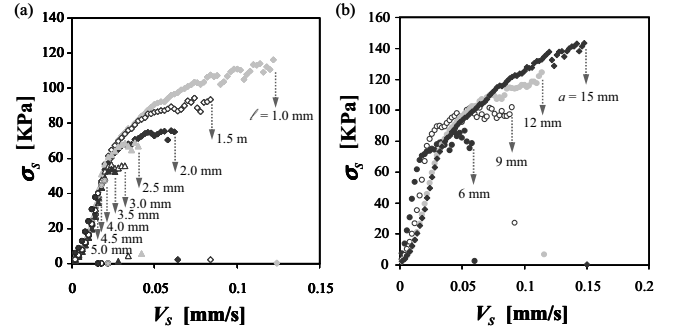


Fig. 8. Shear stress of a silanized glass prism sliding against a thin (300 μ m) PDMS film of modulus 1.6 MPa. In experiments (a) a rectangular glass prism (10 mm \times 10 mm \times 6 mm) was used and the shear force was applied at various heights (ℓ) from the prism/polymer interface. In experiment (b), various glass prisms were used where the value of a varied from 6 mm to 15 mm, but the value of ℓ was kept at 1 mm. Similar experiments were also carried out with the value of ℓ as 2 mm. Arrows represent the stress at which the prism comes off the PDMS film.

a linear combination of $\sigma_n^2 h/\mu$ and $\sigma_s^2 h/\mu$. Equating the total energy release rate to the work of adhesion and making use of equation (14), we get the critical failure shear stress as

$$\sigma_s \cong \frac{a}{\sqrt{(\alpha a^2 + \beta \ell^2)}} \left(\frac{W_a \mu}{h} \right)^{\frac{1}{2}}, \quad (24)$$

where, α and β are numerical constants to be evaluated experimentally. Note that even with the above correction, the dependence of the shear stress on the shear modulus and the thickness of the PDMS film remains unchanged from that shown in equation (17).

According to equation (24), the failure is shear dominated when $\frac{\ell}{a} \sim 0$, but it is normal stress dominated when $\frac{a}{\ell} \sim 0$. In order to simplify the analysis of the experimental data, we rearrange equation (24) as follows:

$$\frac{W_a \mu}{\sigma_s^2 h} = \alpha + \beta \left(\frac{\ell}{a} \right)^2. \quad (25)$$

The shear fracture data shown in Figure 8 (together with some data not shown in Fig. 8) are organized to yield a plot of $W_a \mu/\sigma_s^2 h$ vs. $(\ell/a)^2$ in Figure 9, where the value of the work of adhesion (W_a) is taken to be that (40 mJ/m²) of a typical van der Waals interaction [7]. This plot shows that $W_a \mu/\sigma_s^2 h$ indeed varies linearly with $(\ell/a)^2$ as expected from equation (25). The values of α and β as obtained from Figure 9 are 0.02 and 0.59, respectively. A much smaller value of α compared to β indicates that the shear strain energy release rate is significantly smaller than that due to normal stress, which may be reasonable considering the fact that a significant amount of shear strain energy is used up in the propagation of cavitation bubbles. In view of the fact that $\beta \gg \alpha$, σ_s can be expressed as in equation (26), *i.e.*, the failure is controlled by normal stress as shown in equation (17) so long

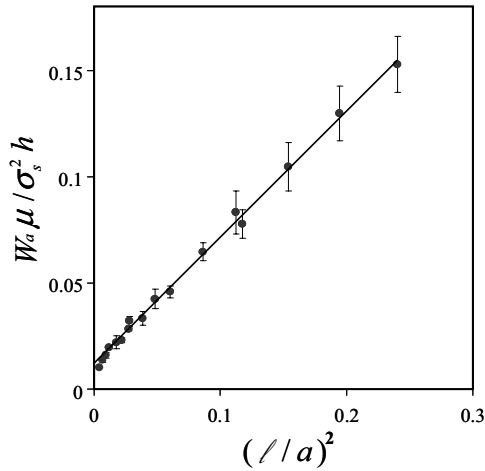


Fig. 9. Dependence of the critical shear stress to failure (σ_s) on the ratio a/ℓ . Correlation co-efficient is 0.99.

as (ℓ/a) is not too small,

$$\sigma_s = 1.30 \left(\frac{a}{\ell}\right) \sqrt{\frac{W_a \mu}{h}}. \quad (26)$$

5 Conclusions

This research sheds some light on the joint roles of shear and normal stresses in the fracture of rigid studs from soft elastomers. While the interfacial friction determines the amount of force needed to cause shear fracture, it occurs when the condition for crack opening is satisfied. The simple model presented here captures the relationship between the shear and normal stress at the interface, predicting the relationship between the critical force of shear fracture with the modulus and thickness of the confined film rather well. The model also accounts for the effect of the external length scales, *i.e.* the length of the prism and the plane of the application of shear stress, on shear fracture reasonably well. An interesting finding of this work is the generation and propagation of bubbles at the interface of the soft film and the rigid slab. These bubbles have the characteristics of interfacial dislocations that originate due to elastic instability and seem to be unique to highly confined systems. A simple energy dissipation argument, in which the driving force of the bubble due to shear energy gradient is balanced by the friction force originating from the cyclic deformation and relaxation of the rubber, gives an approximate description of the bubble motion.

This research was funded by the Office of Naval Research (ONR). The discussions on pages 179 and 180 resulted in response to some comments received from Prof. P.-G. de Gennes, who passed away on May 18. While we are grateful to Late Prof. de Gennes for his insightful comments, we take sole responsibility for any mistakes incurred with the current analysis. We also thank two anonymous referees for their constructive comments that improved the manuscript. The discussion presented on pages 181 and 182 is in response to a valuable suggestion made by one of the referees.

Appendix A. Elastic instability

The wavelength of elastic instability can be estimated using a simple scaling argument [8,9,18] in which we minimize the elastic and surface strain energy (per unit area) of the film:

$$\bar{U}_T \sim \mu h \left[\left(\frac{\partial u}{\partial z} \right)^2 + \left(\frac{\partial w}{\partial x} \right)^2 \right] + \gamma \left(\frac{\partial w}{\partial x} \right)^2, \quad (A.1)$$

where μ , h , and γ are the modulus, thickness, and surface tension of film, and u and w are the components of the displacement field of the films in the x (parallel to the film/prism interface) and z (perpendicular to the film/prism interface) directions, respectively. The contribution of the surface energy in equation (A.1) is very small for elastomers of thickness in the range of micrometers as compared to that of the elastic energy (*i.e.* $\gamma/\mu h < 1$). Thus, we neglect the second term of equation (A.1) in comparison to the elastic strain energy terms. Taking the characteristic length scales as λ and h along the x and z axes, and the amplitude of the perturbation the film as δ , $\partial u/\partial z$ and $\partial w/\partial x$ are on the order of u/h and δ/λ , respectively. However, application of the equation of displacement continuity ($\partial u/\partial x + \partial w/\partial z = 0$) suggests that $u \sim \delta \lambda/h$. Thus the strain energy in the film (Eq. (A.1)) becomes

$$\bar{U}_T \sim \mu h \delta^2 \left[\frac{\lambda}{h^2} + \frac{1}{\lambda} \right]^2. \quad (A.2)$$

Minimization of \bar{U}_T with respect to λ yields $\lambda \sim h$, *i.e.* the wavelength of the instability depends only on the thickness of the film as has been reported in references [16,17]. The linear dependence of λ on h can also be demonstrated more rigorously using a procedure similar to Shenoy and Sharma [30], who analyzed the problem by considering a distance dependent attractive force between the soft film and a rigid contactor. In our case, as the film is separated from the rigid contactor, no long range attractive force operates across the interface. All the interfacial interaction is lumped into work of adhesion, which does not depend on the wavelength of instability. Our problem is thus a simple elastic energy minimization problem. This can be achieved by first solving the biharmonic equation of a stream function and determining the displacement fields from the derivatives of the stream function in conjunction with the following boundary conditions: $u = w = 0$ at the lower surface where the film is bonded to a support and that there is no friction where instability develops at the film/contactor interface.

$$\nabla^4 \phi(x, z) = 0, \quad (A.3)$$

$$u = \frac{\partial \phi}{\partial z} \quad \text{and} \quad w = -\frac{\partial \phi}{\partial x}. \quad (A.4)$$

The normal displacement of the film is the amplitude of instability (δ), which is related to the external stress. To account for elastic instability, equation (A.3) is solved by considering its perturbed form as $\phi(x, z) = \phi(z) \sin kx$. The elastic energy of the film (Eq. (A.1)) can thus be

expressed in dimensionless form as $(\bar{U}_T h / \mu \delta^2) = f(kh)$. When the function $f(kh)$ is determined numerically, it is found to have a minimum at $kh = 2.12$ giving $\lambda \approx 3h$ as was also reported in references [16, 17] using a distance dependent attractive interaction in the overall energy calculation. Experimentally, the wavelength of instability is found to be close to four times the thickness. This discrepancy is due to many simplifications used in our analysis. For example, the problem has to be solved in 3-d instead to 2-d as outlined here. Furthermore, introduction of some friction at the film contactor interface also increases the value of λ closer to $4h$, as has also been noted in a recent report by Adda-Bedia and Mahadevan [31].

Appendix B. Normal force in the film and justifications of equations (13) and (15)

Substitution of $\lambda \sim h$ in equation (A.2) leads to the energy of the film as: $\bar{U}_T \sim \mu \delta^2 / h$ (see also Ref. [17]). Derivative of this energy with respect to normal displacement δ leads to a normal stress $\sigma_n \sim \mu \delta / h$, which can also be written as in equation (B.1) if the amplitude of instability is identified as the normal displacement (v) of the prism/film interface:

$$\sigma_n \sim \mu v / h. \quad (\text{B.1})$$

For a rigid stud with one of its end lifted up, the normal displacement v is linearly proportional to x ; thus the normal stress varies linearly with x as $\sigma_n = \sigma_n^*(x/a)$ (Eq. (13)). The total energy (Eq. (10)) can now be written as

$$U \sim \frac{\mu v_o^2 a}{h} - W_a a. \quad (\text{B.2})$$

Now, setting $\frac{\partial U}{\partial a} \Big|_{v_o} = 0$, and making use of the fact that $\sigma_n^* \sim \mu v_o / h$, we obtain equation (15).

Appendix C. Background of equation (5)

A detailed derivation of equation (5) is given in reference [7]. Briefly, the elasticity equation $[\partial P / \partial x = \mu(\partial^2 u / \partial z^2)]$ within the lubrication approximation is integrated to find an expression for the horizontal displacement (u) in the film in terms of z and h . After substituting this expression for u in the continuity equation $[(\partial u / \partial x + \partial w / \partial z = 0)]$, and integrating $\partial w / \partial z$ along the depth of the film yields an expression for the vertical displacement in the film as shown in equation (5).

References

1. A. Becka, G. Loeb, *Biotechnol. Bioeng.* **26**, 1245 (1984).
2. A.A. Griffith, *Philos. Trans. R. Soc. London, Ser. A* **221**, 163 (1921).
3. R.S. Rivlin, A.G. Thomas, *J. Polym. Sci.* **10**, 291 (1953).
4. A.N. Gent, *Rubber Chem. Technol.* **47**, 202 (1974).
5. K. Kendall, *J. Phys. D: Appl. Phys.* **4**, 1186 (1971).
6. A. Ghatak, L. Mahadevan, J.Y. Chung, M.K. Chaudhury, V. Shenoy, *Proc. R. Soc. London, Ser. A* **460**, 2725 (2004).
7. A. Ghatak, L. Mahadevan, M.K. Chaudhury, *Langmuir* **21**, 1277 (2005).
8. J.Y. Chung, M.K. Chaudhury, *J. Adhes.* **81**, 1119 (2005).
9. J.Y. Chung, K.H. Kim, M.K. Chaudhury, J. Sarkar, A. Sharma, *Eur. Phys. J. E* **20**, 47 (2006).
10. F. Yang, J.C.M. Li, *Langmuir* **17**, 6524 (2001).
11. H. Lakrout, P. Sergot, C. Creton, *J. Adhes.* **69**, 307 (1999).
12. C. Creton, H. Lakrout, *J. Polym. Sci. Part B: Polym. Phys.* **38**, 965 (2000).
13. A.J. Crosby, K.R. Shull, H. Lakrout, C. Creton, *J. Appl. Phys.* **88**, 2956 (2000).
14. R.E. Webber, K.R. Shull, A. Roos, C. Creton, *Phys. Rev. E* **68**, 021805 (2003).
15. A. Ghatak, M.K. Chaudhury, *Langmuir* **19**, 2621 (2003).
16. A. Ghatak, M.K. Chaudhury, V. Shenoy, A. Sharma, *Phys. Rev. Lett.* **85**, 4329 (2000).
17. W. Mönch, S. Herminghaus, *Europhys. Lett.* **53**, 525 (2001).
18. J.Y. Chung, M.K. Chaudhury, *J. R. Soc. Interface* **2**, 55 (2005).
19. A. Ghatak, *Phys. Rev. E* **73**, 041601 (2006).
20. M.K. Chaudhury, M.E. Callow, J.A. Callow, J.A. Finlay, J.Y. Chung, *Biofouling* **21**, 41 (2005). In this paper an experiment was described where a rigid stud was pushed off a thin PDMS film by an air jet. Before the rigid stud came off the film, a crack propagated at the interface in the form of fingering instability.
21. A. Schallmach, *Wear* **17**, 301 (1971).
22. C.J. Rand, A. Crosby, *J. Appl. Phys. Lett.* **89**, 261907 (2006).
23. T. Baumberger, C. Caroli, O. Ronsin, *Phys. Rev. Lett.* **88**, 075509 (2002). Slip pulse is the subject of considerable discussion in the geophysical community. Unfortunately, we could not review this vast field in this paper. Several important papers on the subject are cited at the following website: <http://www.scec.org/research/97research/97riceelastodynamics.html>.
24. T. Baumberger, C. Caroli, *Adv. Phys.* **55**, 279 (2006).
25. F. Brochard-Wyart, P.-G. de Gennes, to be published in *J. Adhes.*
26. K.A. Grosch, *Proc. R. Soc. London, Ser. A* **274**, 21 (1963).
27. Y.B. Chernyak, A.I. Leonov, *Wear* **108**, 105 (1986).
28. K. Vorvolakos, M.K. Chaudhury, *Langmuir* **19**, 6778 (2003).
29. M.E.R. Shanahan, A. Carré, *Langmuir* **11**, 1396 (1995).
30. V. Shenoy, A. Sharma, *J. Mech. Phys. Solids* **50**, 1155 (2002).
31. M. Adda-Bedia, L. Mahadevan, *Proc. R. Soc. London, Ser. A* **462**, 3233 (2006).